coatings

MDPI

Article

Salicylic-Zinc Nanocomposites with Enhanced Antibacterial Activity

Sang Gu Kang [1,*,†], Kyung Eun Lee [1,2], Mahendra Singh [1,*] and Ramachandran Vinayagam [1,*,†]

[1] Department of Biotechnology, Institute of Biotechnology, College of Life and Applied Sciences, Yeungnam University, 280 Daehak-Ro, Gyeongsan 38541, Republic of Korea; keun126@ynu.ac.kr
[2] Stemforce, 313 Institute of Industrial Technology, Yeungnam University, 280 Daehak-Ro, Gyeongsan 38541, Republic of Korea
* Correspondence: kangsg@ynu.ac.kr (S.G.K.); m.singh2685@gmail.com (M.S.); rambio85@gmail.com (R.V.)
† These authors contributed equally to this work.

Abstract: Numerous infectious diseases and microorganisms with high drug resistance have motivated researchers to develop nanocomposite particles as antimicrobial agents. Herein, we report on nanocomposites of salicylic acid (SA) and 5-sulfosalicylic acid (5-SSA) with zinc oxide (ZnO), namely SA-ZnO and 5-SSA-ZnO nanoparticles (NPs), with antibacterial and cytotoxic properties. Ultraviolet-visible and Fourier-transform infrared spectroscopy of the synthesized SA-ZnO and 5-SSA-ZnO NPs indicated the functionalization of ZnO with SA and 5-SSA. X-ray diffraction revealed the crystalline structures of the synthesized NPs. The zeta potentials of the SA-ZnO, 5-SSA-ZnO, and ZnO NPs were 1.42, −5.98, and −0.172, respectively. The SA-ZnO and 5-SSA-ZnO NPs were spherical. Besides, the results of the antimicrobial assay indicated a significant reduction ($p < 0.05$) in the growth of *Escherichia coli* and *Bacillus cereus* by SA-ZnO and 5-SSA-ZnO NPs (0.1%). Scanning electron microscopy of NP-treated bacteria revealed cell death. Moreover, SA-ZnO and 5-SSA-ZnO NPs did not exhibit substantial toxicity against human HaCaT cells even at a high concentration (200 µg/mL). Overall, SA-ZnO and 5-SSA-ZnO NPs exhibited antibiotic-mimicking activity against bacteria with no cytotoxicity.

Keywords: salicylic acid; 5-sulfosalicylic acid; zinc oxide nanoparticles; cosmeceutical; antimicrobial

Citation: Kang, S.G.; Lee, K.E.; Singh, M.; Vinayagam, R. Salicylic-Zinc Nanocomposites with Enhanced Antibacterial Activity. *Coatings* **2023**, *13*, 941. https://doi.org/10.3390/coatings13050941

Academic Editor: Joaquim Carneiro

Received: 2 May 2023
Revised: 13 May 2023
Accepted: 15 May 2023
Published: 17 May 2023

1. Introduction

Nanotechnology is a rapidly developing technology with applications in diagnosis, medicine, cosmetics, environmental science, and other fields [1]. Nanoparticles (NPs) are nanoscale materials, with particle size in the range of 1–100 nm, that have distinct physical and chemical properties [2]. Metal and metal oxide NPs are widely used for the controlled release of specific drugs that protect the skin from ultraviolet light and bacteria [3,4]. Zinc oxide (ZnO) is an important metal oxide with many valuable properties, such as semiconductance and absorption of a wide rangradiationtions. It also exhibits high catalytic activity [5]. ZnO has numerous biotechnological applications in enzyme, agriculture, and textile industries, and is used in various biological techniques [6].

Biodegradable ZnO nanoparticles (ZnO NPs) are often used in cosmetics to protect the skin from harmful radiation [7]. As a modern drug delivery system, ZnO has numerous advantages, including low production costs, biocompatibility, high drug-loading capacity, controllable drug-release ability, and targeted delivery, depending on its size and shape [8]. For instance, ZnO NPs can be used as a photosensitizing agent in sunscreens to protect the skin, and as an antibacterial agent in pharmaceutical industries [9]. Nanocosmetics are formulated using components less than 100 nm in diameter. Owing to its low toxicity, ZnO has been listed as safe by the Food and Drug Administration [10].

High bacterial resistance to conventional antimicrobial drugs has become a global health concern, particularly during the coronavirus disease 2019 (COVID-19) pandemic [11].

Noble metal-doped ZnO NPs can attach to Gram-positive and Gram-negative bacteria via different pathways. The peptidoglycan layer and lipoteichoic acid in the membrane provide negative charges on the cell surface. Using electrostatic interactions, ZnO NPs are attracted to positive charges on the cell surface, which leads to increased cell permeability, damage of membrane proteins, and cell death in microorganisms [12,13]. In addition, ZnO NPs possess antimicrobial activity against human pathogenic bacteria, such as *Streptococcus pneumonia*, *Escherichia coli*, and *Staphylococcus aureus* [14,15]. ZnO NPs have also attracted wide attention owing to their benefits, including antiangiogenic properties and the promotion of the proliferation of adult dermal fibroblasts [16,17]. ZnO NPs functionalized with pomegranate pericarp extract exhibited antimicrobial and antioxidant activities, indicating their potential for biomedical applications [18].

Salicylic acid (SA; 2-hydroxybenzoic acid; $C_7H_6O_3$) is a phenolic acid with an aromatic ring linked to a hydroxyl group that is produced by several plants. 5-Sulfosalicylic acid (5-SSA; with hydroxyl, carboxyl, and sulfonic groups, $C_7H_6O_6S$) is a hydrophilic aromatic compound and one of the most common intermediates in personal care and pharmaceutical products [19]. Numerous studies have examined the antifungal properties of these compounds against various fungi [20,21]. In addition, extensive research has been conducted over the years to uncover the mechanisms of action of SA, and it has been found that SA interferes with the expression of many proinflammatory modulators [22,23]. SA has been shown to reduce endoplasmic reticulum (ER) stress in fibroblasts and adipocytes [24], as well as to reduce skin diseases, including yellow-brownish pigmentation around the eyes [25], and to inhibit tyrosinase activity [26].

SA has been shown to exhibit anticancer effects by inducing ER stress [24]. In addition, a study on the anti-inflammatory effects of SA and aspirin in animal cells showed the inhibition of IκB activity by these compounds [27]. Considering its beneficial properties, SA has been placed under the nonsteroidal anti-inflammatory drug (NSAID) group and is widely used in several cosmetics and medical formulations for skincare products [28]. Owing to its functionality, 5-SSA has been used as a prototype drug that has structural components of several antimicrobial and anti-inflammatory drugs [29].

The uncontrolled use of antibiotics has led to an increase in the growth and spread of antibiotic-resistant microorganisms. Due to the higher rates of resistance and slower pace of development of novel antibiotics, the use of traditional antibiotics to treat bacterial diseases has become more challenging [30]. For instance, methicillin-resistant bacteria are commonly responsible for skin and nosocomial infections in humans [31]. This has raised concerns about a "postantibiotic era" in which many bacterial infections may become incurable [32]. Hence, alternative nonantibiotic therapeutic options have been investigated to ensure that clinicians can access viable medications and evaluate the possible roles of nonconventional and nonantibiotic approaches [33,34]. In this context, nanocomposites or nanomedicines based on natural active substances with improved functional nonantibiotic activity or antibacterial cosmetic agents are important for the treatment of microbial infections.

Here, we report for the first time, the synthesis of SA and 5-SSA NPs with ZnO NPs and the antibacterial effects of these NPs. These compounds were selected because they can increase penetration, improve ingredient stability, and function as active agents. In this study, we focused on the synthesis and physicochemical characterization of SA-ZnO and 5-SSA-ZnO NPs and their antibacterial activity and cytotoxicity.

2. Materials and Methods

2.1. Chemicals and Materials

Human keratinocytes (HaCaT cells) were obtained from American Type Culture Collection (ATCC) (Manassas, VA, USA). Zinc nitrate, SA, 5-SSA, and sodium borohydride. Dulbecco's modified Eagle's medium (DMEM), fetal bovine serum (FBS), 0.25% trypsin-EDTA, and phosphate-buffered saline (PBS) were purchased from Welgene (Gyeongsan, Republic of Korea) and Sigma Aldrich (St. Louis, MO, USA). Penicillin (100 units/mL), streptomycin (100 g/mL), and 3-(4,5-dimethylthiazol-2-yl)-2,5-diphenyltetrazolium bro-

mide (MTT) were obtained from HyClone (Logan, UT, USA). All other chemicals and reagents used in this study were of analytical grade.

2.2. Synthesis and Characterization of SA-ZnO and 5-SSA-ZnO NPs

To prepare SA- and 5-SSA-conjugated ZnO NPs, 1 mL of 1 M zinc nitrate was mixed with 1 mL of 4 M SA and 5-SSA separately and the volume was made up to 100 mL using ddH_2O. Then, 1:4 and 4:1 volume fractions of zinc nitrate were separately prepared with both SA and 5-SSA and incubated at room temperature for 10 min. The solution was heated at 90 °C under magnetic stirring for 30 min and cooled to room temperature, followed by the dropwise addition of 500 µL of sodium borohydride (0.2 M) under vigorous magnetic stirring over an ice bath. The reaction mixture was continuously stirred for the next 4 h. Finally, the NPs were collected by centrifugation at 2500× *g* for 10 min in Figure 1. All samples were dried at 45 °C overnight and stored in an airtight container at room temperature for further analysis. Similarly, ZnO NPs were synthesized without SA or 5-SSA and used as controls for SA-ZnO and 5-SSA-ZnO NPs.

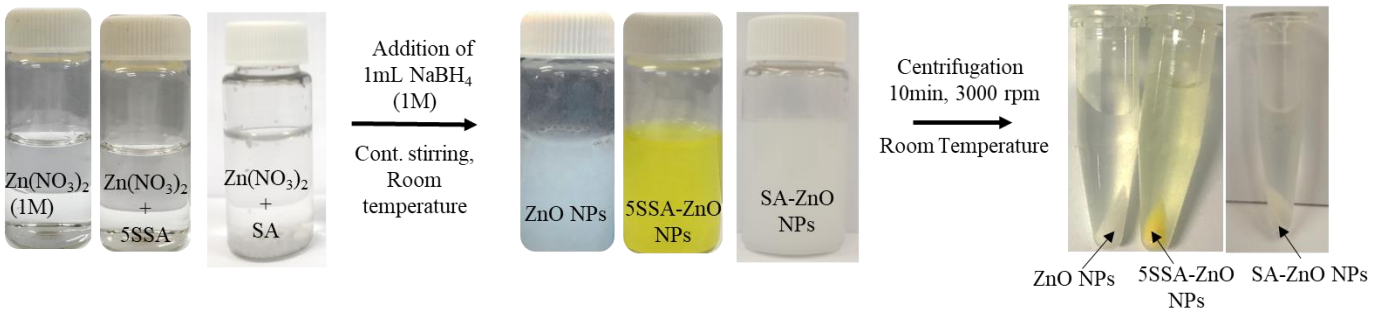

Figure 1. Synthesis scheme and characteristics of Nanocomposites. SA: salicylic acid, 5-SSA:5-sulfosalicylic acid, $Zn(NO_3)_2$:zinc nitrate.

After synthesis, the NPs were characterized using various analytical techniques. The dried samples were examined for NP formation using a UV-Vis spectrophotometer (OPTIZEN 2120UV/VIS, Mecasys, Daejeon, Republic of Korea). The functional groups and binding properties of the NPs were also assessed in terms of transmittance (in the 400–4000 cm^{-1} range) using a Fourier transform-infrared (FTIR) spectrometer (Waltham, MA, USA). SA, 5-SSA, SA-ZnO NPs, and 5-SSA-ZnO NPs were analyzed using powder X-ray diffraction (XRD, MPD, PANalytical) and subjected to particle size analysis (Malvern Panalytical Ltd., Malvern, UK). For scanning electron microscopy (SEM), dried samples (10 mg/mL) of ZnO, SA-ZnO, and 5-SSA-ZnO NPs were dissolved in deionized water, and 10 µL of the sample was further diluted to 1 mL. Thereafter, 20 µL of the diluted sample was dropped on carbon tape stacked over SEM stubs. Finally, the samples were dried at 50 °C and spin-coated with Pt for SEM (Hitachi S-4800, Tokyo, Japan).

2.3. Investigation of Antimicrobial Activity

E. coli (ATCC 15597) and *B. cereus* (ATCC 14579) strains were purchased from ATCC (Manassas, VA, USA) and treated with the synthesized NPs. Briefly, 10 µL of bacterial cultures were added to 10 mL of Luria–Bertani (LB) medium and incubated for 12 h at 37 °C with shaking (120 rpm). Bacterial cells were harvested by centrifugation at 2500× *g* for 10 min. After washing with phosphate-buffered saline (PBS, pH 6.8), the cells were resuspended at a density of 10^4 cells/mL. These cells were inoculated in fresh LB medium mixed with 0.1% of the test samples (SA, 5-SSA, ZnO NPs, SA-ZnO NPs, and 5-SSA-ZnO NPs) and incubated under shaking conditions at 37 °C for 12 h. Subsequently, treated bacterial cultures were serially diluted (10^{-5}, 10^{-6}, and 10^{-7}) and then gently spread on LB agar media plates, and incubated at 32 °C for 12 h [35,36]. Finally, the antibacterial activity of the tested samples was calculated by counting the colonies that emerged on the agar plates.

Similarly, the antibacterial activity assays of ZnO, SA-ZnO, and 5-SSA-ZnO NPs (0.01%) relative to the control (without treatment) were performed for *E. coli* and *B. cereus* and the putative mechanism of bacterial cell destruction was investigated using SEM analysis. Briefly, 10 µL of each bacterial culture was inoculated from broth culture in 10 mL LB medium and incubated for 12 h under shaking conditions (120 rpm) at 37 °C. Bacterial cells were harvested, washed with PBS (pH 6.8), and resuspended at a density of 10^4 cells/mL. These cells were inoculated in fresh LB liquid medium in 96-well plates containing nylon membrane cut into a round shape (diameter, 0.5 cm) and treated with ZnO NPs, SA-ZnO NPs, and 5-SSA-ZnO NPs (0.01% each) or were left untreated (control), and then incubated at 32 °C for 12 h. The cells that adhered to the nylon membrane were fixed with 2.5% *w*/*v* glutaraldehyde and 2% *w*/*v* formaldehyde in PBS. The cells were then dehydrated using an ethanol gradient series (70%, 80%, 100% ethanol) for 10 min at each concentration and subsequently with acetone two to three times. Finally, the washed bacterial cells were dried under a halogen lamp and sputter-coated with gold and palladium. SEM analysis was performed (S-4800, Hitachi, Tokyo, Japan) to observe the structures of the treated and nontreated bacteria.

2.4. Cell Toxicity Profiling

HaCaT cells were cultured in DMEM medium supplemented with 10% FBS, and 100 units/mL each of penicillin and streptomycin in a 5% CO_2 incubator at 37 °C. It was cultured undersupply, and subculturing was performed at 2–3 day intervals. HaCaT cells were uniformly dispensed into a 96-well plate at a density of 1×10^4 cells per well, and then SA-ZnO and 5-SSA-ZnO NPs were added at 25, 50, 100, and 200 µg/mL for 48 h to measure cytotoxicity and proliferation. The Aqueous One Solution Cell Proliferation Assay Kit (Promega, Madison, WI, USA) was used to examine the dose-dependent effects of SA-ZnO and 5-SSA-ZnO NPs on cell proliferation. Thereafter, the old medium was removed, and 100 µL of fresh DMEM and 20 µL MTT solution were added, followed by incubation for 3 h in 5% CO_2 at 37 °C. The sample was kept at room temperature in the dark and the absorbance was measured using an ELISA reader (Infinite^{TM} F200, Tecan, Mannedorf, Switzerland). An untreated culture was used as a control.

2.5. Statistical Analysis

Mean ± S.D. values were calculated using the Statistical Package for the Social Science (SPSS) (version 20, SPSS Inc., New York, NY, USA). The statistical significance of differences between the experimental and control groups was determined using the Student's *t*-test. A *p*-value ≤ 0.05 was considered statistically significant.

3. Results and Discussion

In this era of multidrug-resistant bacterial diseases, novel nonantibiotic therapeutic agents for bacterial infections may provide a means to enhance the effectiveness of existing antibiotics [37]. Metal oxide NPs have been used as therapeutic antibacterial agents [38,39]. Therefore, we developed nonantibiotic cosmeceutical NPs offering the nonsteroidal anti-inflammatory functions of SA and 5-SSA in conjunction with the antibacterial function of ZnO. The SA-ZnO and 5-SSA-ZnO NPs developed in this study have the potential for protecting against bacterial infections.

3.1. UV-Visible Spectroscopy

The synthesis of ZnO NPs was initially confirmed using UV-VIS spectroscopy, with these NPs showing a characteristic absorbance peak at 360 nm. SA, 5-SSA, SA-ZnO NPs, and 5-SSA-ZnO NPs showed an absorption maximum at 300 nm, resulting in an energy band gap (4.1 eV) as calculated using Planck's equation for the preparation of ZnO NPs (Figure 2a). An absorbance peak was found between 300 and 400 nm in an earlier report on the synthesis of ZnO NPs [40]. In another study, a scan of synthesized ZnO NPs in the 200–450 nm wavelength range, revealed an absorbance peak at 360 nm [41]. A

similar absorbance peak was reported in other studies [18,42]. When scanned at the same wavelength, equal concentrations (10 µg/mL) of SA-ZnO and 5-SSA-ZnO NPs showed a reduced peak compared with those of SA and 5-SSA (Figure 2a). From these results, it can be concluded that SA and 5-SSA integrated with the ZnO NPs, resulting in the formation of SA-ZnO and 5-SSA-ZnO NPs.

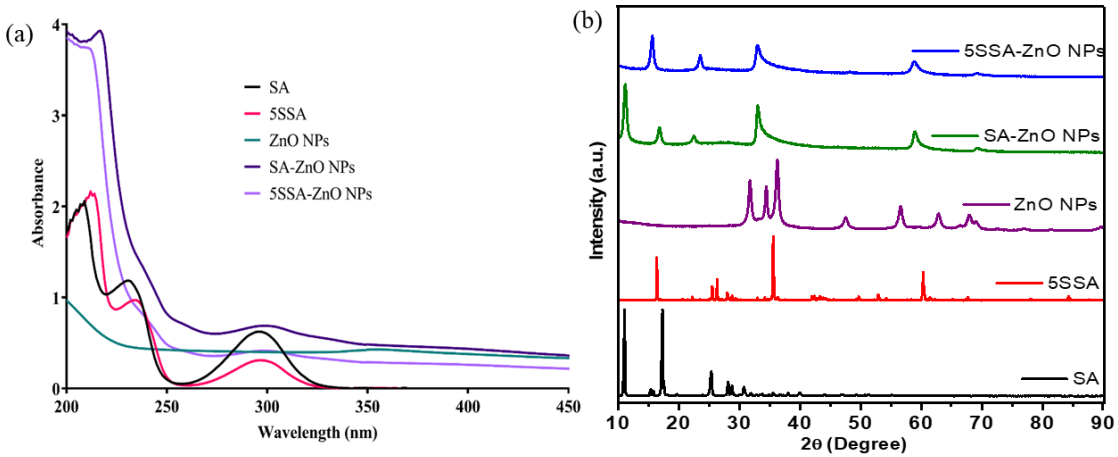

Figure 2. (**a**) UV absorbance spectrum of salicylic acid (SA), 5-sulfosalicylic acid (5-SSA), ZnO nanoparticles (NPs), SA-ZnO NPs, and 5-SSA-ZnO NPs. (**b**) X-ray diffraction (XRD) analysis of SA, 5-SSA, ZnO NPs, SA-ZnO NPs, and 5-SSA-ZnO NPs.

3.2. X-ray Diffraction Analysis of Nanocomposites

The XRD patterns of SA, 5-SSA, ZnO NPs, SA-ZnO NPs, and 5-SSA-ZnO NPs are shown in Figure 2b. For SA, the XRD pattern showed 2θ values at 11.09, 15.40, 17.33, 25.38, 28.13, 30.75, and for SSA, the values were 16.41, 25.52, 26.35, 28.05, 35.60, 52.93, and 60.34. The main peaks of ZnO NPs in XRD patterns revealed 2θ values at 31.71, 34.49, 36.20, 47.47, 56.71, 62.93, and 67.84 for which the reflection was indexed to (100), (002), (101), (102), (110), (103), (112), and (201), respectively. However, as shown in Figure 2b, the XRD pattern of the SA-ZnO NPs shows characteristic peaks at 16.93, 22.49, 33.23, 59.02, 69.40, and that of 5-SSA-ZnO NPs shows peaks at 11.12, 15.67, 23.62, 33.18, 58.94, and 69.34. Upon incorporation of SA and 5-SSA into ZnO NPs, some of the crystalline peaks vanished and ZnO crystalline peaks emerged, revealing the formation of composite SA-ZnO and 5-SSA-ZnO NPs, respectively. In particular, SA-ZnO and 5-SSA-ZnO NPs showed patterns of peaks different from those of ZnO NPs. The average crystallite sizes obtained from the assigned peaks shown in Figure 2b were 15.77, 14.56, and 13.97 nm for ZnO NP, SA-ZnO NPs, and 5-SSA-ZnO NPs, respectively. The XRD pattern clearly indicates the functionalization of ZnO with SA. Furthermore, the narrow diffraction peak revealed the formation of crystalline ZnO NPs [43] that were synthesized using the standard diffraction data for ZnO NPs available in the library (JCPDS 00-036-1451) [44].

3.3. FTIR Spectroscopic Analysis of Nanocomposites

The FTIR spectra were used to identify functional groups associated with SA, 5-SSA, ZnO NPs, SA-ZnO NPs, and 5-SSA-ZnO NPs (Table 1 and Figure 3a). The FTIR spectra of ZnO NPs showed a broad peak assigned to the hydroxyl group with stretching at 3381 cm^{-1}. The C-H bending vibration band was observed at 1382 cm^{-1}. The =C-H bending vibration bands appeared at 903 and 693 cm^{-1}. The spectrum of SA showed peaks at 3230 and 2999 cm^{-1}, which were assigned to O-H and C-H stretching, respectively. The C=O and C=C stretching were assigned to the peaks at 1653 and 1607 cm^{-1}, respectively. The O-H, C-O, and C-OH (phenolic) stretching peaks were observed at 1441, 205–1291, and 1151 cm^{-1}, respectively. The vibration peaks at 886 and 688 cm^{-1} were attributed to C-H and =C-H, respectively. The FTIR spectrum of pure 5-SSA (Table 1) showed the characteristic vibrational peaks of C-H bonds in the benzene ring at 3022 cm^{-1}. The distinct peaks at

1657, 1478, and 1438 cm^{-1} were assigned to C=O, O-H, and COO^- stretching, respectively. The vibrational increase that appeared at 715 cm^{-1} was ascribed to C-H. The composite FTIR spectrum of SA-ZnO showed an intense peak at 560 cm^{-1} due to Zn-C interactions, and the disappearance of the peak at 780 cm^{-1} implied a change from the plane of -OH to $-O^-$ vibrations. The formation and deformation of the peaks confirmed zinc-to-salicylic acid interactions. The broad peak at 3403 cm^{-1} corresponded to the stretching vibrations of the O-H phenol group and the peaks at 1393, 1249, and 1141 cm^{-1} corresponded to the C-H, C-N, and C-O stretching, respectively; the appearance of new peaks at 755 and 655 cm^{-1} corresponded to C=C and that at 655 cm^{-1} corresponded to C=O stretching. For the 5-SSA-ZnO NPs, the peak at 558 cm^{-1} was attributed to the Zn-C interaction. The disappearance of the peak at ~900 cm^{-1} further confirmed the Zn–5-SSA interaction (Figure 3a). The peak at 3400 cm^{-1} was attributed to O-H stretching (phenols). The absorption at 1606, 1470, and 1242 cm^{-1} indicated C=C stretching, C-H bending, and C-OH, respectively. The bands recorded at 1089 and 670 cm^{-1} were attributed to the C-O alcohol and C=C stretching, respectively, as shown in Table 1 and Figure 3a. The presence of capping and stabilization agents, SA and 5-SSA, was confirmed. Figure 3a shows the stretching vibration at a 600–650 cm^{-1} peak appeared to be the characteristic peak for ZnO functional groups. FTIR spectroscopy was used to measure changes in the chemical bonding between Zn NPs and SA-ZnO NPs. 5-SSA-ZnO NPs showed absorption peaks different from those of ZnO NPs. Specific absorption peaks were observed. Therefore, SA-ZnO and 5-SSA-ZnO NPs have different sizes, compositions, and antimicrobial activity.

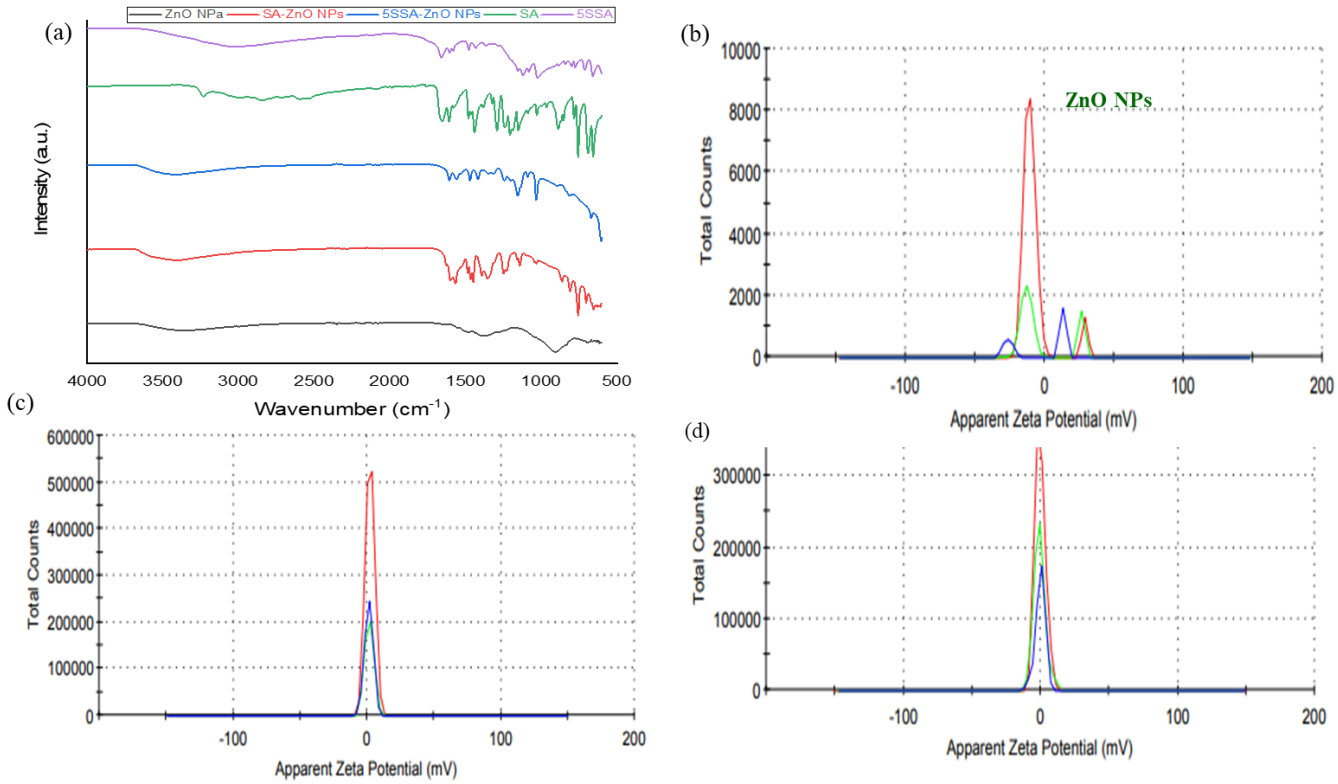

Figure 3. (**a**) The functional groups in SA, 5-SSA, ZnO NPs, SA-ZnO NPs, and 5-SSA-ZnO NPs analyzed using FTIR. (**b–d**) Particle size distribution and zeta potential distribution analysis of ZnO NPs, SA-ZnO NPs, and 5-SSA-ZnO NPs. ZnO NPs: zinc oxide nanoparticles; SA: salicylic acid; 5-SSA:5-sulfosalicylic acid.

Table 1. Fourier-transform infrared (FTIR) frequency range and functional groups present in the samples.

ZnO NPs		SA		5-SSA		SA-ZnO NPs		5-SSA-ZnO NPs	
Wave Number (cm^{-1})	Functional Group	Wave Number (cm^{-1})	Functional Group	Wave Number (cm^{-1})	Functional Group	Wave Number (cm^{-1})	Functional Group	Wave Number (cm^{-1})	Functional Group
3380	O-H	3230	O-H	3022	C-H	3403	O-H	3400	O-H
1382	C-H	2999	C-H	1657	C=C	1599	-N-O	1606	C=C
903	=C-H	1653	C=O	1607	C=C	1484	O-H	1470	C-H
693	=C-H	1607	C=C	1478	O-H	1466	C-H	1242	C-OH
-	-	1441	O-H	1438	COO	1393	C-H	1089	C-O
-	-	1291	C-O	1118	C-O	1249	C-N	1032	C-O
-	-	1205	C-O	1023	S=O	1141	C-OH	670	C=C
-	-	1151	C-OH	715	C-H	755	C=C	558	Zn-C
-	-	886	C-H	655	C=C	655	C=C	900	Zn-O
-	-	688	=C-H	-	-	-	-	-	-
-	-	560	Zn-C	-	-	-	-	-	-
-	-	780	Zn-O		-	-	-	-	-

3.4. Nanostructures of Nanocomposites

Physical and chemical properties, such as surface charge and shape, are critical to the performance of NPs and are responsible for their accumulation at the target site, stability, and circulation [45]. The zeta potential of ZnO NPs was −0.172 mV (Figure 3b), and that of SA-ZnO and 5-SSA-ZnO NPs was 1.42 ± 3.22 and −5.98 mV, respectively (Figure 3c,d). SEM analysis confirmed the shape, size, and structure of ZnO, SA-ZnO, and 5-SSA-ZnO NPs (Figure 4a,e). During the synthesis of ZnO molecules with two different ratios (1:4 and 4:1) of SA and 5-SSA, small spherical structures accumulated. The NPs agglomerated because of the electrostatic attraction between polar ZnO NPs. The synthesized SA-ZnO and 5-SSA-ZnO NPs showed spherical shapes and average particle sizes of 91.82 and 165 nm, respectively (Figure 4b,e,f). However, no significant change was observed upon changing the fraction of zinc salt mixed with SA or 5-SSA. A similar SEM image of spherical particles was reported previously [46,47].

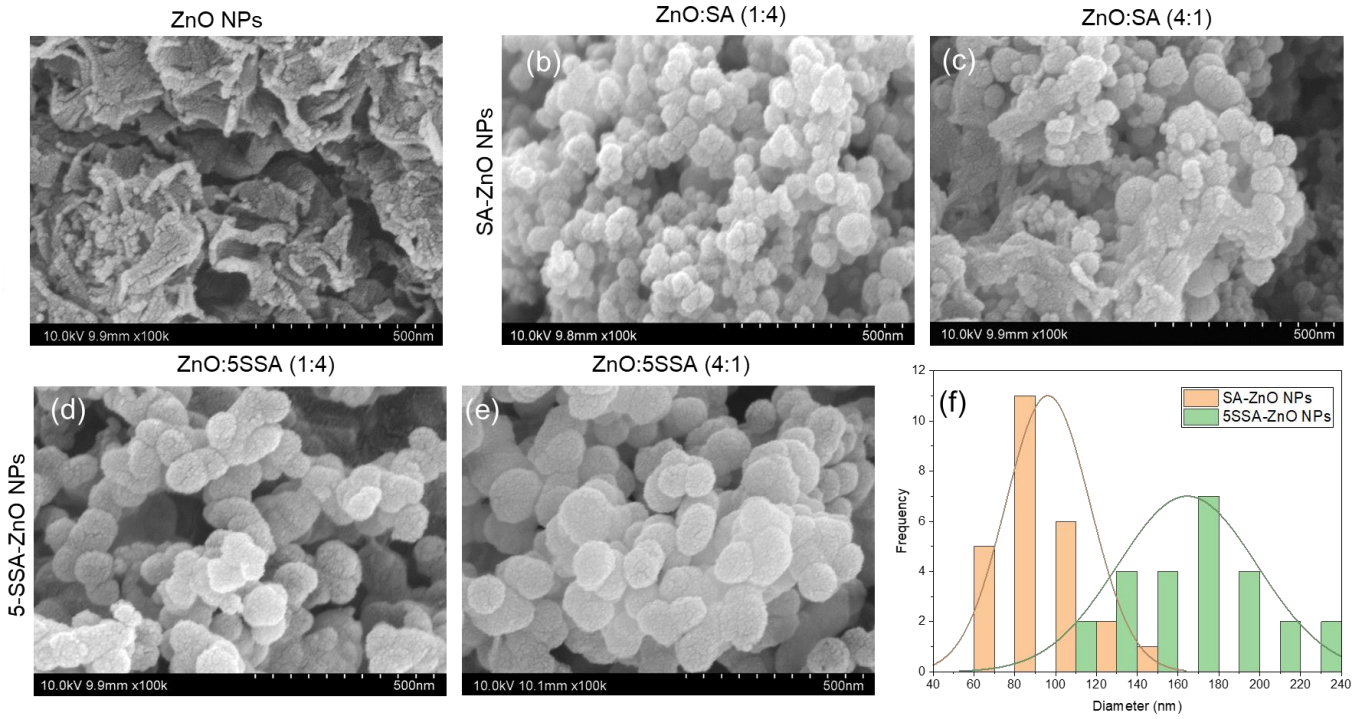

Figure 4. Scanning electron micrographs of nanoparticles. At different ratios (1:4 and 4:1) of ZnO mixed with SA or 5-SSA, ZnO:SA and ZnO:5-SSA NPs of different shapes and sizes were formed. (**a**) ZnO NPs only. (**b**,**c**) SA-ZnO NPs, and (**d**,**e**) 5-SSA-ZnO NPs. (**f**) Particle size distribution. ZnO NPs: zinc oxide nanoparticles; SA: salicylic acid; 5-SSA:5-sulfosalicylic acid.

3.5. Antimicrobial Activity of NPs against E. coli and B. cereus

Recently, inorganic NPs have been effectively utilized in nanobactericidal and nanocarrier strategies for treating diseases and delivering drugs, and they can be used against acute microbial diseases and multidrug-resistant bacterial strains [48,49]. Makabenta et al. reported that ZnO NPs are the next-generation nanoantibiotics that are most commonly investigated against pathogenic/multidrug-resistant microorganisms [1]. We investigated the antimicrobial activity of SA-ZnO and 5-SSA-ZnO NPs against *E. coli* over a concentration range of 0.1–1 mg/mL (0.1%–1%); both the NPs inhibited the growth of *E. coli* (Figure 5a). *B. cereus* is a pathogenic bacterium that causes food poisoning and sepsis. Treatment with 0.1–1 mg/mL (0.1%–1%) of SA-ZnO or 5-SSA-ZnO NPs effectively prevented the growth of this pathogenic bacillus (Figure 5b). Therefore, SA-ZnO and 5-SSA-ZnO NPs may inhibit the growth of a variety of Gram-positive and Gram-negative bacterial species.

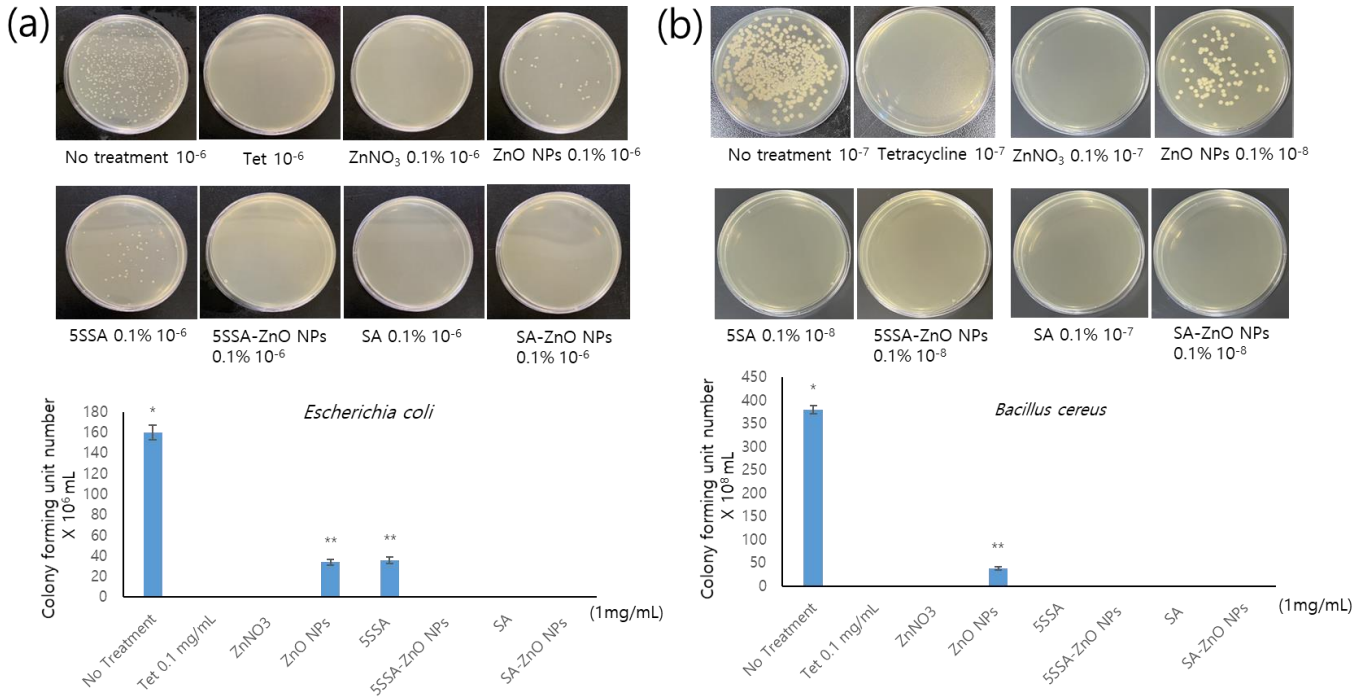

Figure 5. (**a**,**b**) Antimicrobial activity of SA and 5-SSA-ZnO NPs against *Escherichia coli* and *Bacillus cereus*. The colony-forming units (CFU/mL) of bacteria treated with $Zn(NO_3)_2$, SA, 5-SSA, ZnO NPs, SA-ZnO NPs, and 5-SSA-ZnO NPs. $Zn(NO_3)_2$: zinc nitrate; ZnO NPs: zinc oxide nanoparticles; SA: salicylic acid; 5-SSA: 5-sulfosalicylic acid. Results are means ± S.D. of samples. * values are compared with treatment groups, ** values compared with no treatment in the group at $p < 0.05$ Duncan's multiple range test (DMRT).

The antibacterial effects of ZnO, SA-ZnO NPs, and 5-SSA-ZnO NPs with regard to morphological changes in *E. coli* and *B. cereus* were also investigated using SEM. In the no-treatment group, *E. coli* cells had a normal morphology with smooth cellular membranes (Figure 6a). After 1 h of treatment with ZnO NPs (0.01%), initiation of damage to the outer cell membrane was evident (Figure 6b) and after 3 h treatment, extensive damage of *E. coli* cells was observed (Figure 6c). Treatment of bacterial cells with SA-ZnO NPs for 1 h also induced morphological changes (Figure 6e). In contrast, after 3 h of treatment (Figure 6f), bacterial cell damage was enhanced due to the deposition of SA-ZnO NPs (Figure 6e). Treatment of bacterial cells with 5-SSA-ZnO NPs for 1 h resulted in more damage to the outer bacterial cell membrane (Figure 6h) than that observed after 1 h treatment with ZnO and SA-ZnO NPs (Figure 6b,e). After 3 h treatment with 5-SSA-ZnO NPs, the bacterial cell membrane was completely damaged, possibly due to enhanced interaction of 5-SSA-

ZnO NPs with bacterial cell membranes (Figure 6i). Treatment with ZnO, SA-ZnO, and 5-SSA-ZnO NPs for 3 h exhibited strong antibacterial effects against *E. coli*.

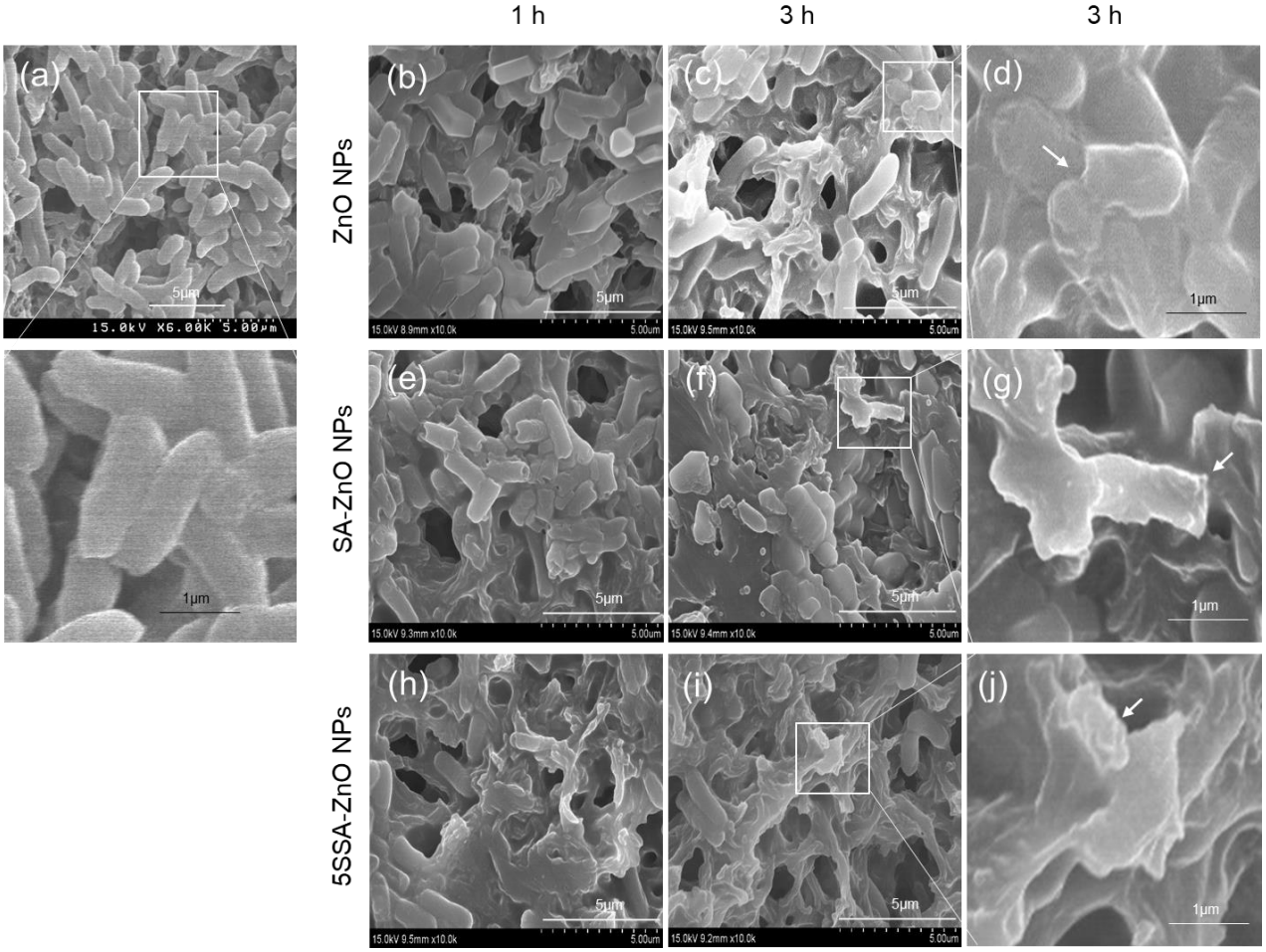

Figure 6. Scanning electron micrographs of *Escherichia coli* either untreated or treated with the synthesized ZnO, SA-ZnO, or 5-SSA-ZnO NPs. (**a**) Control. Treatment with ZnO (0.01%) for 1 h (**b**), ZnO (0.01%) for 3 h (**c**,**d**), SA-ZnO (0.01%) for 1 h (**e**), SA-ZnO (0.01%) for 3 h (**f**,**g**), 5-SSA- ZnO (0.01%) for 1 h (**h**), and 5-SSA- ZnO (0.01%) for 3 h (**i**,**j**). Boxes in (**c**,**f**,**i**) show portions that have been enlarged in (**d**,**g**,**j**), respectively.

Similarly, SEM analysis of *B. cereus* treated with ZnO, SA-ZnO, and 5-SSA-ZnO NPs (0.01% w/v) was performed. Figure 7a shows an SEM image of untreated *B. cereus*; a smooth and intact bacterial membrane surface can be seen in the micrograph. When the cells were treated with ZnO NPs (0.01% w/v) for 1 h, only some morphological changes (membrane corrugation) in the outer membrane of bacteria were seen together with some intact bacteria (Figure 7b); more damage to the outer cell membranes was observed after 3 h, which may be due to the attachment of NPs to cell membranes. Figure 7c shows the image of cells treated with SA-ZnO NPs for 1 h, indicating more severe bacterial destruction than observed after 1 h treatment with ZnO NPs. This could be due to the conjugation of SA with ZnO NPs (Figure 7d). After 3 h of treatment with SA-ZnO NPs, the bacterial cells were destroyed quickly and the cell walls were damaged, which could be responsible for the killing of bacteria (Figure 7f,g). Figure 7e shows the results of 1 h treatment with 5-SSA-ZnO NPs and indicates that bacterial cells may have been killed by corrosion caused by NPs after their attachment to the cells. The 5-SSA-ZnO NPs killed bacterial cells faster than the ZnO and SA-ZnO NPs. Treatment with 5-SSA-ZnO NPs for 3 h (Figure 7i) resulted in almost complete killing of bacteria unlike in the case of treatment with ZnO NPs (Figure 7j).

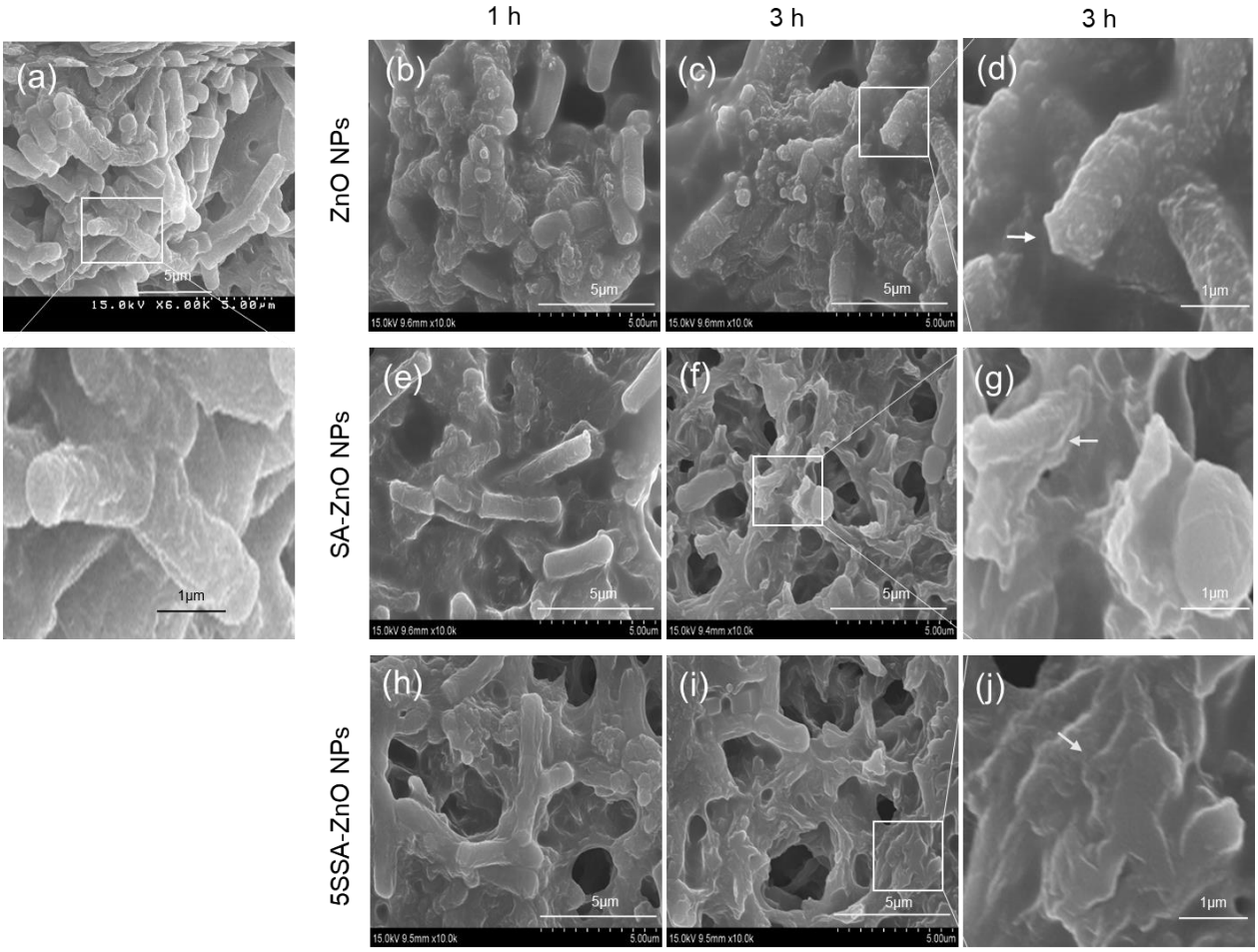

Figure 7. Scanning electron micrographs showing the morphology of *Bacillus cereus* either untreated or treated with the synthesized ZnO, SA-ZnO, or 5-SSA-ZnO NPs. (**a**) Control. Treatment with ZnO (0.01%) for 1 h (**b**), ZnO (0.01%) for 3 h (**c**,**d**), SA-ZnO (0.01%) for 1 h (**e**), SA-ZnO (0.01%) for 3 h (**f**,**g**), 5-SSA-ZnO (0.01%) for 1 h (**h**), and 5-SSA- ZnO (0.01%) for 3 h (**i**,**j**). Boxes in (**c**,**f**,**i**) show portions that have been enlarged in (**d**,**g**,**j**), respectively.

ZnO NPs exhibit considerable bactericidal activity against various infections. Because microbes have a negative charge and ZnO NPs have a positively charged group, an electrostatic interaction occurs between the microbes and the NPs [50]. Once the response is initiated, the microbes are oxidized, resulting in the adherence of the NPs to the bacterial cell wall [51]. In addition, ZnO NPs facilitate access to inactive proteins and bacteria via the microbial cell membrane [52]. Furthermore, there are various mechanisms by which ZnO NPs generate reactive oxygen species (ROS) and hydrogen peroxide, resulting in the inhibition of DNA replication, membrane damage, increased cell permeability, and destruction of bacterial cells [52,53]. Thus, the antibacterial activity of ZnO NPs makes them excellent candidates for use as antibacterial agents against microbes. Furthermore, as evident from the results of SEM analysis in the present study, 3 h treatment with ZnO, SA-ZnO, and 5-SSA-ZnO NPs induced changes in *E. coli* and *B. cereus* cells, such as the disruption of the outer cell membrane (Figures 6 and 7). Based on these findings, the antibacterial effect of SA-ZnO and 5-SSA-ZnO NPs appears to involve increased cell permeability through the disruption of the cell membrane, deformation of bacterial cells, and ROS formation, allowing the leakage of intracellular material, resulting in cell membrane shrinkage and eventually cell death.

As confirmed using FTIR analysis, the novel ZnO NPs in which SA or 5-SSA was conjugated during synthesis, had more phytophenolics that could contribute carboxyl to

the hydroxyl group in the ZnO NPs. Therefore, SA-ZnO and 5-SSA-ZnO NPs may have caused the instability and destruction of the biomolecules in the bacterial cell membrane. In another study, SA and other phytochemicals were shown to have antibacterial activities against *E. coli* and *S. aureus* [54]. It has also been reported that 5 mM salicylate exerts a strong bacteria effect against *E. coli* [55]. Therefore, SA-ZnO NPs and 5-SSA-ZnO NP-mediated bacterial cell death may be influenced by the membrane permeability of *E. coli*, a Gram-negative bacterium. *B. cereus*, a Gram-positive bacterium, was subjected to SEM analysis. Gram-positive bacteria have a thicker peptidoglycan layer than Gram-negative bacteria, which could necessitate more NPs to penetrate the cells [56–58].

3.6. Growth and Proliferation of HaCaT Cells Treated with SA-ZnO or 5-SSA-ZnO NPs

Sunscreens containing ZnO NPs have more advantages over other lotions because of their transparent nature and ability to reflect solar radiation, which prevents skin irritation and photoaging [59,60]. In this study, we performed a cytotoxicity assay to determine the toxicity or protective effects of the NPs on HaCaT cells. At high concentration, ZnO NPs were relatively toxic to HaCaT cells (Figure 8). Additionally, when SA-ZnO and 5-SSA-ZnO NPs were added at a high concentration (200 µg/mL), the growth of the cells was not significantly different from that of the untreated control (Figure 8). Notably, ZnO NPs showed cell toxicity with increasing ZnO NP concentrations. Thus, this study proves that zinc and SA are less toxic when converted into SA-ZnO or 5-SSA-ZnO NPs. This may be because SA and 5-SSA cover the ZnO cores; hence, SA ZnO and 5-SSA-ZnO NPs circumvent the direct contact of ZnO cores with HaCaT cells, resulting in less toxicity. Several studies have suggested that SA exerts its anti-inflammatory activity by inhibiting the transcription of proinflammatory proteins [61] and by absorbing UV radiation [62,63]. Topical application of sodium salicylate shows photoprotective activity, and SA has been shown to reduce skin erythema in mice [64]. This suggests that SA-ZnO and 5-SSA-ZnO NPs confer enhanced antimicrobial activities to cosmetics and pharmaceuticals.

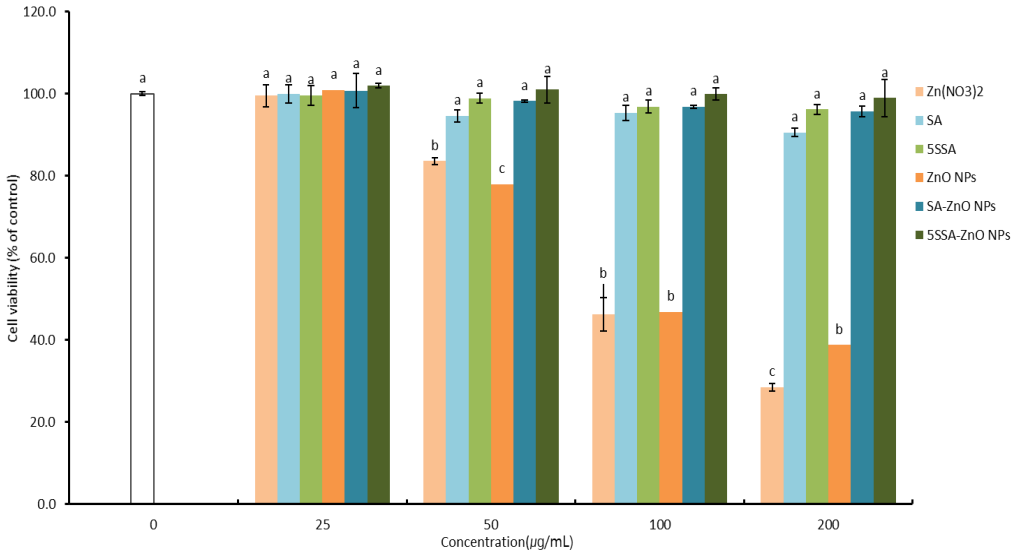

Figure 8. Effect of SA-ZnO and 5-SSA-ZnO NPs on the viability of human HaCaT cells. The cells were treated with $Zn(NO_3)_2$, SA, 5-SSA, ZnO NPs, SA-ZnO NPs, and 5-SSA-ZnO NPs (25, 50, 100, and 200 µg/mL, respectively) for 24 h and then subjected to an MTT assay. Values are means ± S.D. ^{a,b,c} values not sharing a common letter are significantly different among the group at $p < 0.05$ (DMRT).

4. Conclusions

The novel SA-ZnO and 5-SSA-ZnO NPs exhibited potential antibacterial activities. The formation of ZnO NPs was confirmed based on the characteristic peak in the UV-Vis spectra. The SEM images of the SA-ZnO and 5-SSA-ZnO NPs confirmed the structure of the agglomerated irregular or spherical NPs. SA-ZnO NPs exhibited physicochemical proper-

ties different from those of ZnO and SA. SA-ZnO and 5-SSA-ZnO NPs were not cytotoxic to human keratinocytes (HaCaT cells), which indicates the safety of these NPs. Moreover, the nonantibiotic antibacterial activities of SA-ZnO and 5-SSA-ZnO NPs effectively inhibited the growth of pathogenic *E. coli* and *B. cereus*. The novel SA-ZnO and 5-SSA-ZnO NPs may be applied as multitarget antimicrobial agents and can be used in a wide range of UV sunscreens. SA-ZnO and 5-SSA-ZnO NPs can also be used in public health approaches to control pathogenic microorganisms and prevent infectious diseases.

Author Contributions: S.G.K.: Methodology development, supervision, financial support, review, and editing; K.E.L.: In vitro studies and data curation; M.S.: experiments; R.V.: data analysis and writing—original draft preparation. All authors have read and agreed to the published version of the manuscript.

Funding: This work was supported by "LINC+ (Leaders in INdustry-University Co-operation +)" funded by the Ministry of Education, Republic of Korea (2021-D-G043-010115).

Institutional Review Board Statement: Not applicable.

Informed Consent Statement: Not applicable.

Data Availability Statement: Not applicable.

Acknowledgments: The authors thank the Core Research Support Center for Natural Products and Medical Materials at Yeungnam University, Gyeongsan, Republic of Korea, for technical support with the physicochemical investigation using FTIR (PerkinElmer, Inc., Waltham, MA, USA) and Zetasizer Nano ZS (Malvern Panalytical Ltd., Malvern, UK).

Conflicts of Interest: The authors declare no conflict of interest.

References

1. Makabenta, J.M.V.; Nabawy, A.; Li, C.-H.; Schmidt-Malan, S.; Patel, R.; Rotello, V.M. Nanomaterial-based therapeutics for antibiotic-resistant bacterial infections. *Nat. Rev. Microbiol.* **2021**, *19*, 23–36. [CrossRef] [PubMed]
2. Baig, N.; Kammakakam, I.; Falath, W. Nanomaterials: A review of synthesis methods, properties, recent progress, and challenges. *Mater. Adv.* **2021**, *2*, 1821–1871. [CrossRef]
3. Pan, S.; Goudoulas, T.B.; Jeevanandam, J.; Tan, K.X.; Chowdhury, S.; Danquah, M.K. Therapeutic Applications of Metal and Metal-Oxide Nanoparticles: Dermato-Cosmetic Perspectives. *Front. Bioeng. Biotechnol.* **2021**, *9*, 724499. [CrossRef] [PubMed]
4. Vinayagam, R.; Lee, K.E.; David, E.; Matin, M.N.; Kang, S.G. Facile green preparation of PLGA nanoparticles using wedelolactone: Its cytotoxicity and antimicrobial activities. *Inorg. Chem. Commun.* **2021**, *129*, 108583. [CrossRef]
5. Kołodziejczak-Radzimska, A.; Jesionowski, T. Zinc oxide—From synthesis to application: A review. *Materials* **2014**, *7*, 2833–2881. [CrossRef]
6. Sirelkhatim, A.; Mahmud, S.; Seeni, A.; Kaus, N.H.M.; Ann, L.C.; Bakhori, S.K.M.; Hasan, H.; Mohamad, D. Review on zinc oxide nanoparticles: Antibacterial activity and toxicity mechanism. *Nano-Micro Lett.* **2015**, *7*, 219–242. [CrossRef]
7. Niska, K.; Zielinska, E.; Radomski, M.W.; Inkielewicz-Stepniak, I. Metal nanoparticles in dermatology and cosmetology: Interactions with human skin cells. *Chem. Biol. Interact.* **2018**, *295*, 38–51. [CrossRef]
8. Anjum, S.; Hashim, M.; Malik, S.A.; Khan, M.; Lorenzo, J.M.; Abbasi, B.H.; Hano, C. Recent Advances in Zinc Oxide Nanoparticles (ZnO NPs) for Cancer Diagnosis, Target Drug Delivery, and Treatment. *Cancers* **2021**, *13*, 4570. [CrossRef]
9. Sharma, R.; Garg, R.; Kumari, A. A review on biogenic synthesis, applications and toxicity aspects of zinc oxide nanoparticles. *EXCLI J.* **2020**, *19*, 1325.
10. Abdussalam-Mohammed, W. Comparison of chemical and biological properties of metal nanoparticles (Au, Ag), with metal oxide nanoparticles (ZnO-NPs) and their applications. *Adv. J. Chem. Sect. A* **2020**, *3*, 192–210.
11. Hu, X.-Y.; Logue, M.; Robinson, N. Antimicrobial resistance is a global problem–A UK perspective. *Eur. J. Integr. Med.* **2020**, *36*, 101136. [CrossRef] [PubMed]
12. Liu, J.; Wang, Y.; Ma, J.; Peng, Y.; Wang, A. A review on bidirectional analogies between the photocatalysis and antibacterial properties of ZnO. *J. Alloys Compd.* **2019**, *783*, 898–918. [CrossRef]
13. Mendes, C.R.; Dilarri, G.; Forsan, C.F.; Sapata, V.d.M.R.; Lopes, P.R.M.; de Moraes, P.B.; Montagnolli, R.N.; Ferreira, H.; Bidoia, E.D. Antibacterial action and target mechanisms of zinc oxide nanoparticles against bacterial pathogens. *Sci. Rep.* **2022**, *12*, 2658. [CrossRef]
14. Sharifi, S.; Fathi, N.; Memar, M.Y.; Hosseiniyan Khatibi, S.M.; Khalilov, R.; Negahdari, R.; Zununi Vahed, S.; Maleki Dizaj, S. Anti-microbial activity of curcumin nanoformulations: New trends and future perspectives. *Phytother. Res.* **2020**, *34*, 1926–1946. [CrossRef] [PubMed]

15. Gao, Y.; Arokia Vijaya Anand, M.; Ramachandran, V.; Karthikkumar, V.; Shalini, V.; Vijayalakshmi, S.; Ernest, D. Biofabrication of zinc oxide nanoparticles from Aspergillus niger, their antioxidant, antimicrobial and anticancer activity. *J. Clust. Sci.* **2019**, *30*, 937–946. [CrossRef]
16. Meyer, K.; Rajanahalli, P.; Ahamed, M.; Rowe, J.J.; Hong, Y. ZnO nanoparticles induce apoptosis in human dermal fibroblasts via p53 and p38 pathways. *Toxicol. Vitr.* **2011**, *25*, 1721–1726. [CrossRef]
17. Mohammad, G.R.K.S.; Tabrizi, M.H.; Ardalan, T.; Yadamani, S.; Safavi, E. Green synthesis of zinc oxide nanoparticles and evaluation of anti-angiogenesis, anti-inflammatory and cytotoxicity properties. *J. Biosci.* **2019**, *44*, 30. [CrossRef]
18. Singh, M.; Lee, K.E.; Vinayagam, R.; Kang, S.G. Antioxidant and Antibacterial Profiling of Pomegranate-pericarp Extract Functionalized-zinc Oxide Nanocomposite. *Biotechnol. Bioprocess Eng.* **2021**, *26*, 728–737. [CrossRef]
19. Xiao, G.; Wen, R.; Wei, D. Effects of the hydrophobicity of adsorbate on the adsorption of salicylic acid and 5-sulfosalicylic acid onto the hydrophobic-hydrophilic macroporous polydivinylbenzene/polymethylacrylethylenediamine IPN. *Fluid Phase Equilibria* **2016**, *421*, 33–38. [CrossRef]
20. da Rocha Neto, A.C.; Maraschin, M.; Di Piero, R.M. Antifungal activity of salicylic acid against Penicillium expansum and its possible mechanisms of action. *Int. J. Food Microbiol.* **2015**, *215*, 64–70. [CrossRef]
21. Li, L.; Zhu, T.; Song, Y.; Feng, L.; Kear, P.J.; Riseh, R.S.; Sitohy, M.; Datla, R.; Ren, M. Salicylic acid fights against Fusarium wilt by inhibiting target of rapamycin signaling pathway in Fusarium oxysporum. *J. Adv. Res.* **2021**, *39*, 1–13. [CrossRef] [PubMed]
22. Zhang, T.; Sun, L.; Liu, R.; Zhang, D.; Lan, X.; Huang, C.; Xin, W.; Wang, C.; Zhang, D.; Du, G. A novel naturally occurring salicylic acid analogue acts as an anti-inflammatory agent by inhibiting nuclear factor-kappaB activity in RAW264. 7 macrophages. *Mol. Pharm.* **2012**, *9*, 671–677. [CrossRef] [PubMed]
23. Sinha, P.; Srivastava, N.; Rai, V.K.; Mishra, R.; Ajayakumar, P.V.; Yadav, N.P. A novel approach for dermal controlled release of salicylic acid for improved anti-inflammatory action: Combination of hydrophilic-lipophilic balance and response surface methodology. *J. Drug Deliv. Sci. Technol.* **2019**, *52*, 870–884. [CrossRef]
24. Ausina, P.; Branco, J.R.; Demaria, T.M.; Esteves, A.M.; Leandro, J.G.B.; Ochioni, A.C.; Mendonça, A.P.M.; Palhano, F.L.; Oliveira, M.F.; Abou-Kheir, W. Acetylsalicylic acid and salicylic acid present anticancer properties against melanoma by promoting nitric oxide-dependent endoplasmic reticulum stress and apoptosis. *Sci. Rep.* **2020**, *10*, 1–15. [CrossRef]
25. How, K.N.; Lim, P.Y.; Wan Ahmad Kammal, W.S.L.; Shamsudin, N. Efficacy and safety of Jessner's solution peel in comparison with salicylic acid 30% peel in the management of patients with acne vulgaris and postacne hyperpigmentation with skin of color: A randomized, double-blinded, split-face, controlled trial. *Int. J. Dermatol.* **2020**, *59*, 804–812. [CrossRef]
26. Dahl, A.; Yatskayer, M.; Raab, S.; Oresajo, C. Tolerance and efficacy of a product containing ellagic and salicylic acids in reducing hyperpigmentation and dark spots in comparison with 4% hydroquinone. *J. Drugs Dermatol.* **2013**, *12*, 52–58.
27. Yin, M.-J.; Yamamoto, Y.; Gaynor, R.B. The anti-inflammatory agents aspirin and salicylate inhibit the activity of IκB kinase-β. *Nature* **1998**, *396*, 77–80. [CrossRef]
28. Wu, K.K. Salicylates and their spectrum of activity. *Anti-Inflamm. Anti-Allergy Agents Med. Chem. (Former. Curr. Med. Chem. Anti-Inflamm. Anti-Allergy Agents)* **2007**, *6*, 278–292. [CrossRef]
29. Chowdhury, N.A.; Robertson, J.; Jumaily, A.A.; Ramos, M.V. Controlled Release of Sulfosalicylic Acid from Regenerated Cellulose/Functionalized Carbon Nanofibers/Polypyrrole Matrices. *Int. J. Mater. Chem.* **2014**, *4*, 101–108.
30. Yang, X.; Ye, W.; Qi, Y.; Ying, Y.; Xia, Z. Overcoming Multidrug Resistance in Bacteria Through Antibiotics Delivery in Surface-Engineered Nano-Cargos: Recent Developments for Future Nano-Antibiotics. *Front. Bioeng. Biotechnol.* **2021**, *9*, 696514. [CrossRef]
31. Rybak, M.J.; LaPlante, K.L. Community-associated methicillin-resistant Staphylococcus aureus: A review. *Pharmacother. J. Hum. Pharmacol. Drug Ther.* **2005**, *25*, 74–85. [CrossRef] [PubMed]
32. Ruiz, J.; Castro, I.; Calabuig, E.; Salavert, M. Non-antibiotic treatment for infectious diseases. *Rev. Esp. Quimioter.* **2017**, *1*, 66–71.
33. Czaplewski, L.; Bax, R.; Clokie, M.; Dawson, M.; Fairhead, H.; Fischetti, V.A.; Foster, S.; Gilmore, B.F.; Hancock, R.E.W.; Harper, D. Alternatives to antibiotics—A pipeline portfolio review. *Lancet Infect. Dis.* **2016**, *16*, 239–251. [CrossRef]
34. Brooks, B.D.; Brooks, A.E. Therapeutic strategies to combat antibiotic resistance. *Adv. Drug Deliv. Rev.* **2014**, *78*, 14–27. [CrossRef] [PubMed]
35. Muflikhun, M.A.; Frommelt, M.C.; Farman, M.; Chua, A.Y.; Santos, G.N.C. Structures, mechanical properties and antibacterial activity of Ag/TiO2 nanocomposite materials synthesized via HVPG technique for coating application. *Heliyon* **2019**, *5*, e01475. [CrossRef] [PubMed]
36. Parthiban, E.; Manivannan, N.; Ramanibai, R.; Mathivanan, N. Green synthesis of silver-nanoparticles from Annona reticulata leaves aqueous extract and its mosquito larvicidal and anti-microbial activity on human pathogens. *Biotechnol. Rep.* **2019**, *21*, e00297. [CrossRef] [PubMed]
37. Worthington, R.J.; Melander, C. Combination approaches to combat multidrug-resistant bacteria. *Trends Biotechnol.* **2013**, *31*, 177–184. [CrossRef]
38. Zaidi, S.; Misba, L.; Khan, A.U. Nano-therapeutics: A revolution in infection control in post antibiotic era. *Nanomed. Nanotechnol. Biol. Med.* **2017**, *13*, 2281–2301. [CrossRef]
39. Srinivasan, S.; Ramachandran, V.; Murali, R.; Vinothkumar, V.; Raajasubramanian, D.; Kanagalakshimi, A. Biogenic Metal Nanoparticles and Their Antimicrobial Properties. In *Nanotechnological Approaches in Food Microbiology*; CRC Press: Boca Raton, FL, USA, 2020; pp. 403–413.

40. Aldalbahi, A.; Alterary, S.; Ali Abdullrahman Almoghim, R.; Awad, M.A.; Aldosari, N.S.; Fahad Alghannam, S.; Nasser Alabdan, A.; Alharbi, S.; Ali Mohammed Alateeq, B.; Abdulrahman Al Mohsen, A. Greener synthesis of zinc oxide nanoparticles: Characterization and multifaceted applications. *Molecules* **2020**, *25*, 4198. [CrossRef]
41. Muhammad, W.; Ullah, N.; Haroon, M.; Abbasi, B.H. Optical, morphological and biological analysis of zinc oxide nanoparticles (ZnO NPs) using *Papaver somniferum* L. *RSC Adv.* **2019**, *9*, 29541–29548. [CrossRef]
42. Ding, X.; Lin, K.; Li, Y.; Dang, M.; Jiang, L. Synthesis of biocompatible zinc oxide (ZnO) nanoparticles and their neuroprotective effect of 6-OHDA induced neural damage in SH-SY 5Y cells. *J. Clust. Sci.* **2020**, *31*, 1315–1328. [CrossRef]
43. Sundrarajan, M.; Ambika, S.; Bharathi, K. Plant-extract mediated synthesis of ZnO nanoparticles using Pongamia pinnata and their activity against pathogenic bacteria. *Adv. Powder Technol.* **2015**, *26*, 1294–1299. [CrossRef]
44. Ahmad, M.; Rehman, W.; Khan, M.M.; Qureshi, M.T.; Gul, A.; Haq, S.; Ullah, R.; Rab, A.; Menaa, F. Phytogenic fabrication of ZnO and gold decorated ZnO nanoparticles for photocatalytic degradation of Rhodamine B. *J. Environ. Chem. Eng.* **2021**, *9*, 104725. [CrossRef]
45. Wu, T.; Tang, M. Review of the effects of manufactured nanoparticles on mammalian target organs. *J. Appl. Toxicol.* **2018**, *38*, 25–40. [CrossRef] [PubMed]
46. Gandhi, P.R.; Jayaseelan, C.; Mary, R.R.; Mathivanan, D.; Suseem, S.R. Acaricidal, pediculicidal and larvicidal activity of synthesized ZnO nanoparticles using Momordica charantia leaf extract against blood feeding parasites. *Exp. Parasitol.* **2017**, *181*, 47–56. [CrossRef] [PubMed]
47. Rajapriya, M.; Sharmili, S.A.; Baskar, R.; Balaji, R.; Alharbi, N.S.; Kadaikunnan, S.; Khaled, J.M.; Alanzi, K.F.; Vaseeharan, B. Synthesis and characterization of zinc oxide nanoparticles using Cynara scolymus leaves: Enhanced hemolytic, antimicrobial, antiproliferative, and photocatalytic activity. *J. Clust. Sci.* **2020**, *31*, 791–801. [CrossRef]
48. Gupta, A.; Mumtaz, S.; Li, C.-H.; Hussain, I.; Rotello, V.M. Combatting antibiotic-resistant bacteria using nanomaterials. *Chem. Soc. Rev.* **2019**, *48*, 415–427. [CrossRef]
49. Vinayagam, R.; Santhoshkumar, M.; Lee, K.E.; David, E.; Kang, S.G. Bioengineered gold nanoparticles using Cynodon dactylon extract and its cytotoxicity and antibacterial activities. *Bioprocess Biosyst. Eng.* **2021**, *44*, 1253–1262. [CrossRef]
50. Xu, J.; Huang, Y.; Zhu, S.; Abbes, N.; Jing, X.; Zhang, L. A review of the green synthesis of ZnO nanoparticles using plant extracts and their prospects for application in antibacterial textiles. *J. Eng. Fibers Fabr.* **2021**, *16*, 15589250211046242. [CrossRef]
51. Ahmed, B.; Ameen, F.; Rizvi, A.; Ali, K.; Sonbol, H.; Zaidi, A.; Khan, M.S.; Musarrat, J. Destruction of cell topography, morphology, membrane, inhibition of respiration, biofilm formation, and bioactive molecule production by nanoparticles of Ag, ZnO, CuO, TiO_2, and Al_2O_3 toward beneficial soil bacteria. *ACS Omega* **2020**, *5*, 7861–7876. [CrossRef]
52. Gudkov, S.V.; Burmistrov, D.E.; Serov, D.A.; Rebezov, M.B.; Semenova, A.A.; Lisitsyn, A.B. A Mini Review of Antibacterial properties of ZnO nanoparticles. *Front. Phys.* **2021**, *9*, 641481. [CrossRef]
53. Karnwal, A.; Kumar, G.; Pant, G.; Hossain, K.; Ahmad, A.; Alshammari, M.B. Perspectives on Usage of Functional Nanomaterials in Antimicrobial Therapy for Antibiotic-Resistant Bacterial Infections. *ACS Omega* **2023**, *8*, 13492–13508. [CrossRef] [PubMed]
54. Monte, J.; Abreu, A.C.; Borges, A.; Simões, L.C.; Simões, M. Antimicrobial activity of selected phytochemicals against Escherichia coli and Staphylococcus aureus and their biofilms. *Pathogens* **2014**, *3*, 473–498. [CrossRef] [PubMed]
55. Blaskovich, M.A.T.; Elliott, A.G.; Kavanagh, A.M.; Ramu, S.; Cooper, M.A. In vitro antimicrobial activity of acne drugs against skin-associated bacteria. *Sci. Rep.* **2019**, *9*, 1–8. [CrossRef]
56. Ahluwalia, V.; Elumalai, S.; Kumar, V.; Kumar, S.; Sangwan, R.S. Nano silver particle synthesis using Swertia paniculata herbal extract and its antimicrobial activity. *Microb. Pathog.* **2018**, *114*, 402–408. [CrossRef]
57. Fang, G.; Li, W.; Shen, X.; Perez-Aguilar, J.M.; Chong, Y.; Gao, X.; Chai, Z.; Chen, C.; Ge, C.; Zhou, R. Differential Pd-nanocrystal facets demonstrate distinct antibacterial activity against Gram-positive and Gram-negative bacteria. *Nat. Commun.* **2018**, *9*, 129. [CrossRef]
58. Maruthupandy, M.; Rajivgandhi, G.; Muneeswaran, T.; Song, J.-M.; Manoharan, N. Biologically synthesized zinc oxide nanoparticles as nanoantibiotics against ESBLs producing gram negative bacteria. *Microb. Pathog.* **2018**, *121*, 224–231. [CrossRef]
59. Chauhan, R.; Kumar, A.; Tripathi, R.; Kumar, A. Advancing of zinc oxide nanoparticles for cosmetic applications. In *Handbook of Consumer Nanoproducts*; Springer: Berlin/Heidelberg, Germany, 2022; pp. 1–16.
60. Smijs, T.G.; Pavel, S. Titanium dioxide and zinc oxide nanoparticles in sunscreens: Focus on their safety and effectiveness. *Nanotechnol. Sci. Appl.* **2011**, *4*, 95–112. [CrossRef]
61. Amann, R.; Peskar, B.A. Anti-inflammatory effects of aspirin and sodium salicylate. *Eur. J. Pharmacol.* **2002**, *447*, 1–9. [CrossRef]
62. Weirich, E.G.; Longauer, J.K.; Kirkwood, A.H. Dermatopharmacology of salicylic acid. *Dermatology* **1975**, *151*, 321–332. [CrossRef]
63. Kristensen, B.; Kristensen, O. Topical salicylic acid interferes with UVB therapy for psoriasis. *Acta Derm. Venereol.* **1991**, *71*, 37–40. [PubMed]
64. Bair, W.B.; Hart, N.; Einspahr, J.; Liu, G.; Dong, Z.; Alberts, D.; Bowden, G.T. Inhibitory effects of sodium salicylate and acetylsalicylic acid on UVB-induced mouse skin carcinogenesis. *Cancer Epidemiol. Prev. Biomark.* **2002**, *11*, 1645–1652.